Köppen–Geiger Climate Classification for Europe Recaptured via the Hölder Regularity of Air Temperature Data

Adrien Deliège & Samuel Nicolay

Pure and Applied Geophysics
pageoph

ISSN 0033-4553
Volume 173
Number 8

Pure Appl. Geophys. (2016)
173:2885-2898
DOI 10.1007/s00024-016-1339-3

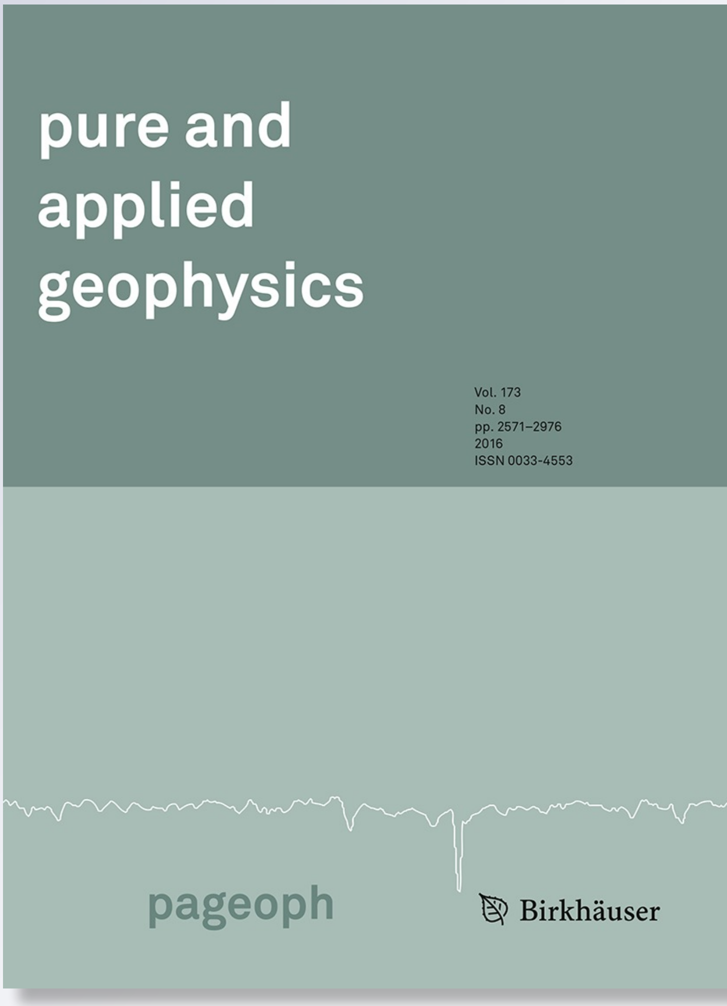

Pure Appl. Geophys. 173 (2016), 2885–2898

DOI 10.1007/s00024-016-1339-3

Pure and Applied Geophysics

Köppen–Geiger Climate Classification for Europe Recaptured via the Hölder Regularity of Air Temperature Data

ADRIEN DELIÈGE[1] and SAMUEL NICOLAY[1]

Abstract—In this paper, we make use of the monoHölder nature of surface air temperature data to recapture the Köppen–Geiger climate classification in Europe. Using data from the European Climate Assessment and Dataset (ECA&D), we first show that the Hölder exponents of surface air temperature data are statistically related to pressure anomalies. Then, we establish a climate classification based on these Hölder exponents in such a way that it allows to recover the Köppen–Geiger climate classification. We show that the two classifications match for a vast majority of stations, and we corroborate these observations with a confirmation test. We compare these results with those obtained with another dataset (NCEP-NCAR Reanalysis Project) to show that the new classification is still well-adapted, before eventually discussing these findings.

Key words: Surface air temperature, Hölder regularity, Köppen–Geiger classification.

1. Introduction

This work explores the notion of Hölder regularity of surface air temperature data in Europe. It has been shown that, from a Hölder point of view, air temperature data displays a "regularly irregular" (monoHölder) behavior [e.g., Koscielny-Bunde et al. (1998); Sonechkin and Datchenko (2000)], which can roughly be described as follows. We say that a signal f is associated with the Hölder exponent h_{t_0} at t_0 if $|f(t) - f(t_0)|$ behaves like the power law $|t - t_0|^{h_{t_0}}$ if t is close enough to t_0. If the function $t_0 \mapsto h_{t_0}$ is constant, the signal is said to be monoHölder. The Hölder exponent of a monoHölder signal represents its "regularity", i.e., it gives a global characterization of the variations within the signal: the higher the Hölder exponent, the most regular the signal (Mandelbrot and Van Ness 1968). This is illustrated in Fig. 1, where three monoHölder functions with different Hölder exponents are represented. One can clearly see that the signals become less irregular as their Hölder exponent increases.

Among the numerous efficient ways to determine the Hölder exponent of a signal, the Wavelet Leaders Method (WLM) is a recent and mathematically sound tool [see e.g., Jaffard (2004); Jaffard et al. (2006); Jaffard and Nicolay (2009) for mathematical details]. The idea is to use a particular function, called wavelet (Daubechies 1992; Mallat 1999), as a microscope to analyze the signal at different scales (Arneodo et al. 1995; Muzy et al. 1994). One of the main advantages of this method as other wavelet-based methods, comes from the fact that it can be used on the raw data and that is not "bias-dependent", i.e., it is not sensitive to polynomial trends (Arneodo et al. 1995, 2011; Audit et al. 2002). The WLM has already demonstrated its astounding usefulness in several scientific fields, such as fully developed turbulence (Lashermes et al. 2008), heart rate variability (Abry et al. 2010) and texture classification (Wendt et al. 2009). It is thus natural to try to apply this method to the analysis of climate data.

We apply this formalism in climatology with European surface air temperature data with two questions in mind. The first one is: is there a strong connection between Hölder exponents and standard deviations of air pressure anomalies? Indeed, the variability in pressure anomalies can intuitively be seen as a natural indicator of the regularity of the climate type that a given region withstands. The second question is: is the Hölder exponent of a given surface air temperature time series a possible characteristic of its associated climate type? As shown in

[1] University of Liège, Liège, Belgium. E-mail: adrien.deliege@ulg.ac.be; s.nicolay@ulg.ac.be

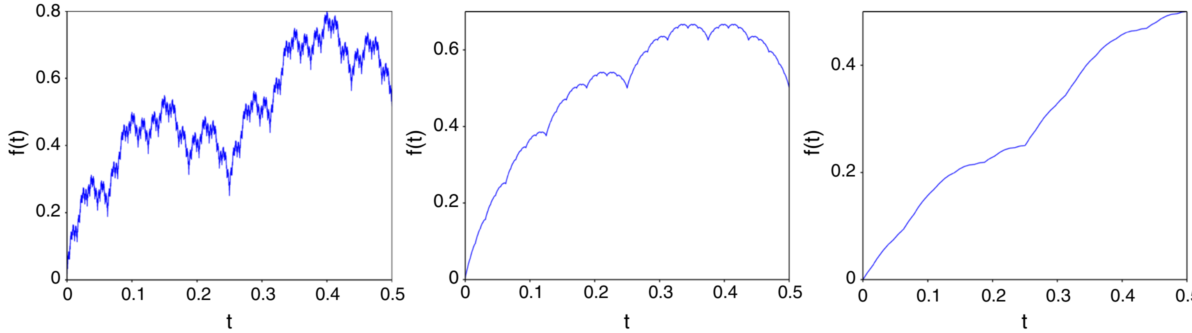

Figure 1
Three monoHölder functions of the same type [Takagi functions, see Allaart and Kawamura (2011); Shidfar and Sabetfakhri (1986); Tricot (1999)], with Hölder exponent 0.5, 1, and 1.5. One can clearly see that the regularity of the signal increases with the Hölder exponent

this paper, it turns out that the Hölder exponents of air temperature data in Europe are indeed closely linked with the Köppen–Geiger climate classification system (Köppen 1936; Peel et al. 2007).

The rest of this work is structured as follows. In Sect. 2, we describe the dataset used and the main ideas of the WLM. Then, in Sect. 3, we exhibit a strong anti-correlation between Hölder exponents and standard deviations of air pressure anomalies and give a statistical validation of this feature. In Sect. 4, we establish a climate classification based on the Hölder exponents in such a way that it allows to recover a simplified version of the Köppen–Geiger classification for Europe. We show that the two classifications match for almost all the stations, and we perform a confirmation test to sustain these observations. We compare these results with those obtained with another dataset to show that the new classification is still well-adapted. Section 5 is devoted to the discussion of the results. Finally, we summarize our results in Sect. 6 and we give insights on possible future work. It is worth to add that, to the best of our knowledge, it is the first time that these experiments are conducted this way. In particular, we found no trace in the scientific literature of prior attempts to recapture locally the Köppen classification from Hölder exponents.

2. Data and Method

2.1. Data

The surface air temperature data used throughout this paper was downloaded from the European Climate Assessment and Dataset website (ECA&D) (http://ecad.eu) and consists of daily mean temperatures. Stations were selected in Europe in an area delimited by parallels 36°N (which includes Spain, Italy, Greece) and 55°N (Ireland, Germany) and meridians 10°W (Ireland, Portugal) and 40°E (Ukraine) to have a consistent geographic zone and limit the effects of latitude. Also, stations located above 1000 m of altitude were first removed to prevent altitude from interfering with the results, and only data between years 1951 and 2003 were analyzed in order to have numerous homogeneous data. As a result, it appeared that 115 stations fulfilled these requirements. Moreover, the standard deviations of pressure anomalies used in Sect. 3, computed from 1951 to 2003, were provided by the NCEP-NCAR Reanalysis Project (http://www.esrl.noaa.gov/). The surface air temperature data used in Sect. 4.3 to compare the results with another dataset are also provided by the NCEP-NCAR Reanalysis Project (http://www.esrl.noaa.gov/).

2.2. The Wavelet Leaders Method

We briefly recall the principle of the WLM used to compute the Hölder exponents of the stations; the interested reader can refer to Jaffard and Nicolay (2009) for more details. First, we perform the wavelet decomposition of the signal:

$$f(x) = \sum_{j,k \in \mathbb{Z}} c_{j,k} \psi(2^j x - k) = \sum_{\lambda \in \Lambda} c_\lambda \psi_\lambda ,$$

where ψ is the wavelet and $c_{j,k}$ is the wavelet coefficient associated with the dyadic interval λ at the scale j and position k: $\lambda = \lambda_{j,k} = [2^{-j}k, 2^{-j}(k+1)[$ and

$$c_{j,k} = 2^j \int_{\mathbb{R}} f(x)\psi(2^j x - k)dx.$$

Then, for each λ, we compute the wavelet leaders

$$d_\lambda = \sup_{\lambda' \subset \lambda} |c_{\lambda'}|.$$

We remove the null wavelet leaders and compute

$$S(q,j) = \frac{1}{2^j} \sum_{\lambda \in \Lambda_j} d_\lambda^q,$$

where Λ_j is the set of dyadic intervals at scale j. We finally compute the function τ defined as

$$\tau(q) = \underline{\lim}_{j \to +\infty} \frac{\log(S(q,j))}{\log 2^{-j}}.$$

A linear function τ is the signature of a monoHölder function and its slope is the Hölder exponent.

Since a monoHölder function belongs to a uniform Hölder space, one can associate the following norm to f: $N = \max_{j,k}\{|c_{j,k}|/2^{jh}\}$. Note also that the air temperature data are "integrated" before the WLM analysis, i.e., the n-th value was replaced by the sum of the first n values (Riley et al. 2012). This was performed in order to have more stable numerical results; it also explains why the Hölder exponents obtained are greater than 1 compared to other results obtained in the literature. The wavelet chosen for the analyses is the second-order Daubechies wavelet, but the results do not differ when using other orders.

3. Anti-correlation Between Hölder Exponents and Pressure Anomalies

We first examine the relation between Hölder exponents and pressure anomalies. The estimation of the Hölder exponents via the WLM is illustrated in Fig. 2 for the air temperature data of Brindisi (the same linear trend is observed for all the stations) and the norms are computed as described in the previous section. The distribution of these parameters is represented in Fig. 3.

Each station is associated with its Hölder exponent h_n and its inverse of the standard deviation of pressure anomalies p_n $(n = 1, \ldots, 115)$. In order to

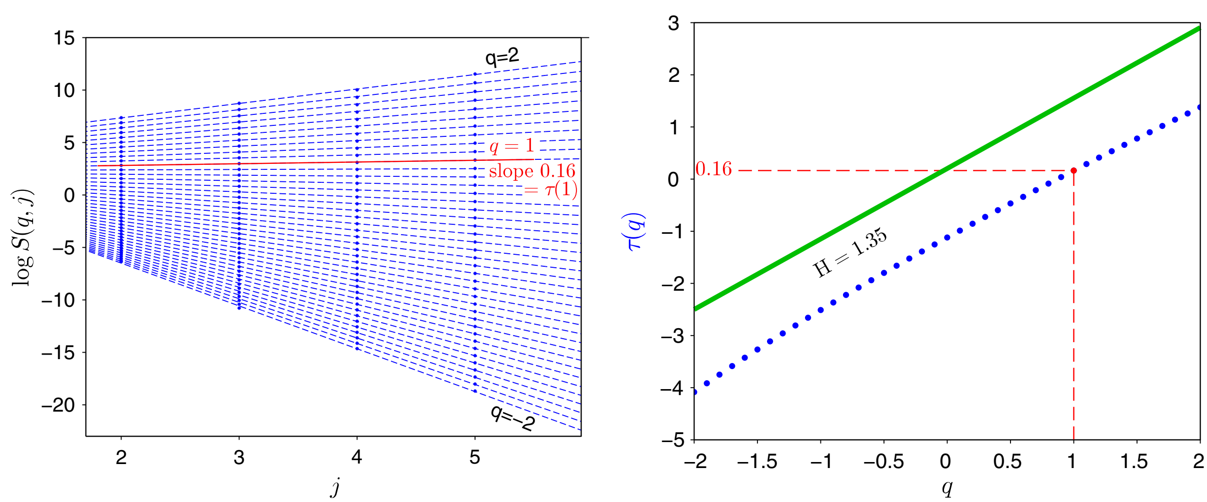

Figure 2

Estimation of the Hölder exponent for Brindisi (Italy). *Left* $\log(S(q,j))$ versus j for $q = -2$ to $q = 2$ (increasing by step 0.1) and their associated linear regression lines (*dashed blue lines*). For each value of q, the value of $\tau(q)$ is computed as the slope of the linear regression of $j \mapsto \log(S(q,j))$. This is illustrated for $q = 1$ (*red*). *Right* τ versus q (*blue*) and associated linear regression line (*green*) with a vertical shift for the sake of clarity. Since τ displays a linear behavior (linear correlation coefficient greater than 0.99), the slope of the regression line gives the Hölder exponent H of the signal

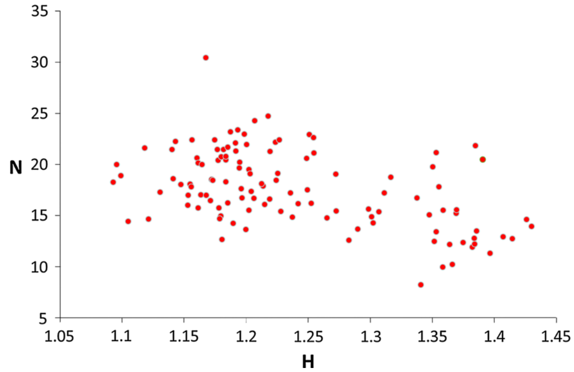

Figure 3
Distribution of the Hölder exponents and norms of the air temperature datasets

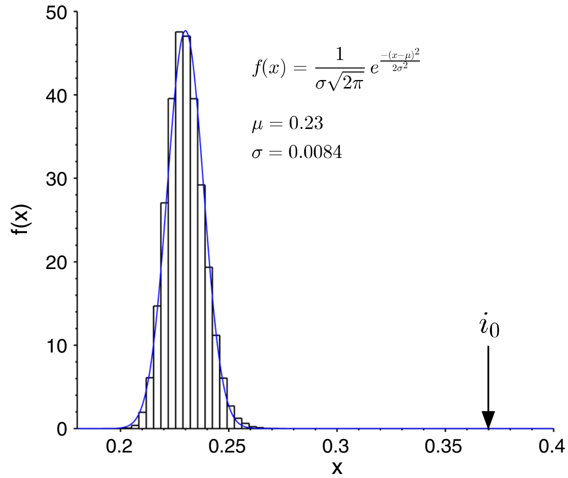

Figure 4
The *blue* curve is the Gaussian curve with mean $\mu = 0.23$ and standard deviation $\sigma = 0.0084$ related to the underlying histogram of the indices of similarity i_m ($m = 1, \ldots, 100{,}000$) between random shuffles of the "Hölder exponents series" h_n ($n = 1, \ldots, 115$) and the "inverse of pressure anomalies series" p_n. The *arrow* represents the measured index of similarity $i_0 = 0.37$ between the original series h_n and p_n. Obviously, the probability to measure such a large index i_0 is extremely low, which indicates that Hölder exponents and standard deviation of pressure anomalies are anti-correlated

measure if these two series are close, we first normalize them, i.e., h_n becomes

$$\frac{h_n - \max_n\{h_n\}}{\max_n\{h_n\} - \min_n\{h_n\}}$$

(and similarly for p_n). Then we compute the Euclidean distance between them, i.e., the value

$$d = \sqrt{\sum_{n=1}^{115} (h_n - p_n)^2},$$

and we define $i_0 = d^{-1}$ as an index of similarity between them. In this case, the value of i_0 obtained is $i_0 = 0.37$.

To check if this index is statistically significant, we compute the same distance but with a randomly shuffled series h_n to obtain the index of similarity i_1. We iterate the process 100,000 times to obtain the indices i_m ($m = 1, \ldots, 100{,}000$). Statistical tests accept the hypothesis that they are normally distributed, with mean $\mu = 0.23$ and standard deviation $\sigma = 0.0084$ (see Fig. 4). This implies that the probability that a random shuffle of the Hölder series gives an index of similarity larger than i_0 is of order 10^{-50}, which means that i_0 is a highly significant index of similarity. Therefore the anti-correlation between the Hölder exponents and the standard deviation of pressure anomalies is confirmed: the higher the standard deviation of pressure anomalies, the lower the Hölder exponents.

4. *From Hölder Exponents to a Climate Classification*

4.1. *Köppen–Geiger Climate Classification*

In order to link the Hölder exponents of the stations displayed in Fig. 3 with their associated climate, we determine the climate type of each station according to a simplified version of the Köppen–Geiger climate classification (Köppen 1936; Peel et al. 2007). Although precipitation is part of the original classification, we do not take it into account since we focus on air temperature variability. By doing so, and considering the area in which the stations were selected, only two parameters remain to determine the climate type of a station: minimum (m) and maximum (M) monthly mean temperatures. These induce four different types of climate: Mediterranean (Ca-type, $m > 0\,°C$, $M > 22\,°C$), Oceanic (Cb-type, $m > 0\,°C$, $M < 22\,°C$), Hot continental (Da-type, $m < 0\,°C$, $M > 22\,°C$), Temperate continental (Db-type, $m < 0\,°C$, $M < 22\,°C$) (see Fig. 5).

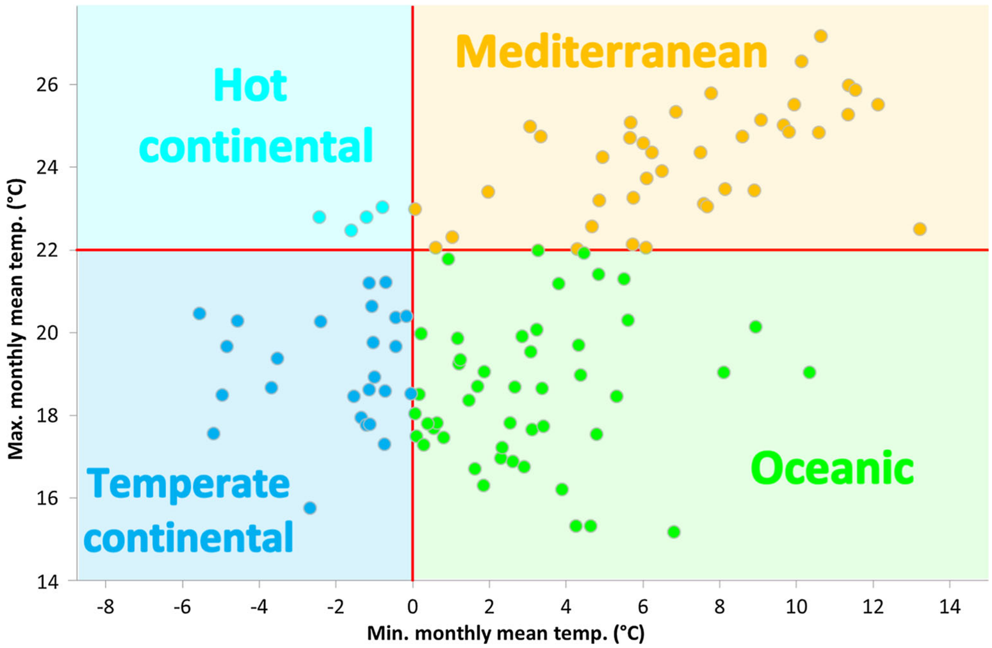

Figure 5

Distribution of the 115 weather stations within the different climate types in Europe, according to a simplified version of the Köppen–Geiger climate classification: in this case, precipitation is not taken into account. Hot continental and temperate continental climates are merged and considered as continental climate. Stations close to 0.5 °C of another type of climate are also associated with this second category

Considering as references the Köppen classification and the map of Europe presented in Peel et al. (2007), our simplification has the effect of merging similar climate types. More precisely, the large part of Spain originally classified as an arid cold steppe (BSk-type, mainly defined by very low precipitation) is now under the Mediterranean label, as well as Northern Italy and some parts of the Balkans (e.g., Serbia), which display the Cfa-type (same as Mediterranean climate with a wetter summer). They clearly have common features in their air temperature data with the surrounding Mediterranean regions and it is thus reasonable to merge them in the present work. Similarly, the Csb-type (mainly the North part of Portugal) has now the Oceanic tag since they only differ by the amount of precipitation during summer. Finally, the cold continental types (Dsa, Dfc and ET) only occur at high altitude in the selected area of Europe; data from weather stations located above 1000 m of altitude will be discussed separately. Subsequently, one can see that neglecting precipitation leads to a union of similar climate types in a consistent way. In Europe, the main interest of taking precipitation into account is to differentiate some relatively small regions of the South half of the continent from the surrounding areas. This somehow brings more diversity in the climate classification, though air temperature remains the most significant and discriminant parameter. Besides, the intrinsic nature of precipitation measurements make it irrelevant to use techniques such as the WLM to extract valuable information.

As a last remark, stations close to 0.5 °C of another type of climate are also associated with this second category. This is justified by the fact that climate may change over time; indeed, 12.2 % of the stations display a different climate type when computed from 1951 to 1977 and from 1977 to 2003. Also, due to the lack of Da-type stations (in Europe, only found around the Black Sea), hot continental and temperate continental classes are merged into one category, i.e., Continental stations (D-type). The climate distribution among the stations is given by Fig. 6.

4.2. A Hölder Exponents-Based Climate Classification

To check if the Köppen–Geiger climate classification in Europe can be regained from the Hölder analysis, we plot the points cloud representing the Hölder exponents (abscissa) and norms (ordinate) of the stations, where each point is colored according to its climate type (see Fig. 7). Since points with the same color are concentrated in the same areas, one may try to cut the plane into rectangles to isolate the three climates. A simple possibility is to use only two vertical cuts (let us say at H_1 and H_2) and two horizontal cuts (let us say at N_1 and N_2), which gives 9 rectangles. Each of them is then associated with the climate type that is the most abundant therein, which gives rise to a new kind of climate classification. The best way to do so, i.e., the cut-out that gives the maximum coherence between this "Hölder-based classification" and the Köppen–Geiger climate classification, corresponds to the cuts where $H_1 = 1.186$, $H_2 = 1.275$, $N_1 = 14.81$ and $N_2 = 16.18$, which induces the classification given by Table 1. In this case, 93.9 % of the stations are correctly classified, i.e., their Köppen climate type is recovered (see Fig. 7).

We then perform a blind test on other weather stations in the same area to validate the Hölder-based

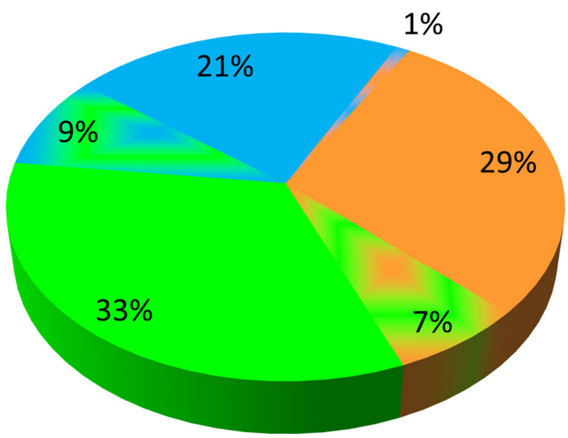

Figure 6
Climate distribution among the 115 weather stations. *Green* (Oceanic, Cb): 33 %, *Orange* (Mediterranean, Ca): 29 %, *Blue* (continental, D): 21 %, Cb and D: 9 %, Ca and Cb: 7 %, Ca and D: 1 %

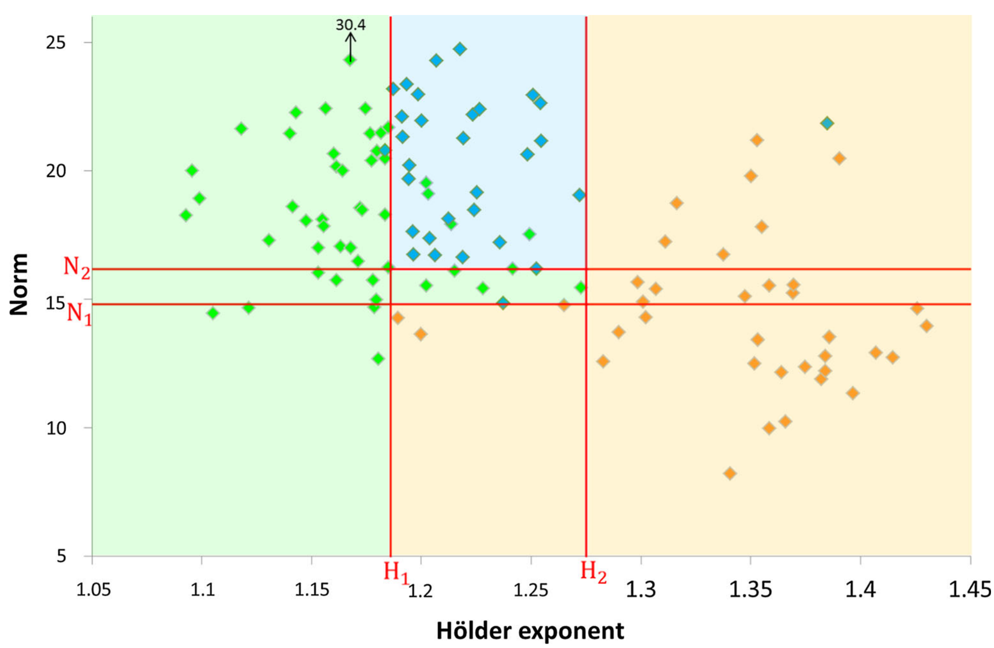

Figure 7
The *diamonds* (*Green* Cb, *Orange* Ca, *Blue* D) represent the distribution of the Hölder exponents and norms of the 115 weather stations. Based on these two variables, the *red lines* cut the plane into *rectangles* that induce a climate classification (given by the *color of the rectangles*) designed to match as much as possible with the Köppen–Geiger classification. Almost 94 % of the points have the same color as the rectangle in which they are located, which indicates that the classification based on Hölder exponents and norms matches with Köppen's

Table 1

The "Hölder-based" climate classification that best matches with Köppen's: almost 94 % of the stations are correctly associated with their climate type

Hölder exponent	Norm	Climate type
$H < 1.186$	All	Oceanic
$1.186 \leq H < 1.275$	$N < 14.81$	Mediterranean
	$14.81 \leq N < 16.18$	Oceanic
	$16.18 \leq N$	Continental
$1.275 \leq H$	All	Mediterranean

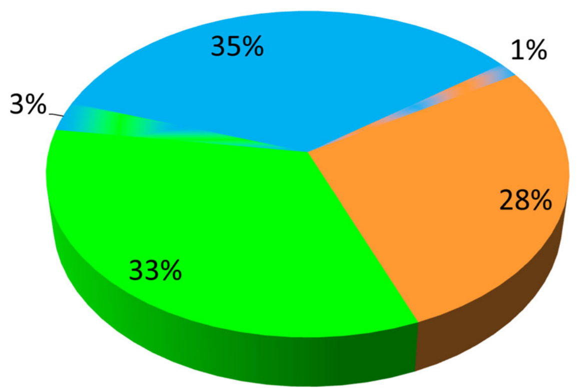

Figure 8
Climate distribution among the 69 weather stations selected for the blind test. *Green* (Oceanic, Cb): 33 %, *orange* (Mediterranean, Ca): 28 %, *blue* (continental, D): 35 %, Cb and D: 3 %, Ca and D: 1 %

classification. Since almost none of the remaining stations available on http://ecad.eu displayed at least 50 years of data between 1951 and 2003, we allowed shorter time series for the test (at least 40 years of data in that period). We found 69 stations exploitable for this experiment. As previously, we determine their Köppen climate types (their distribution is given by Fig. 8) and we plot the points cloud representing the Hölder exponents and norms of these new stations (see Fig. 9). Of course, the values of H_1, H_2, N_1 and N_2 are left unchanged, as well as the cut-out of the plane into rectangles and the colors of these rectangles. In this context, it appears that most of the points (88.4 %) are still correctly classified. Figure 10 shows a global overview of the results (the first 115 stations and the 69 new ones).

As a reminder, all the stations used so far are placed below 1000 m of altitude. One can thus wonder how Hölder exponents behave for weather stations located at high altitudes. We managed to find 10 stations above 1000 m of altitude in the selected part of Europe which display at least 40 years of data between 1951 and 2003. These stations, as well as the associated information (Köppen climate, altitude) and results (Hölder exponent, norm, prescribed climate) can be found in Table 2. Let us remark that according to the simplified version of the Köppen classification described in this paper, these stations are unsurprisingly classified as "Db" (Continental), and none of them is 0.5° close to another type of climate. Nevertheless, following the original classification, Fichtelberg, Mont Aigoual and Zavizan are actually "Dc" type (minimum monthly mean temperature below 0 °C and only between 1 and 3 months display a monthly mean temperature above 10 °C), whereas Sonnblick, Säntis, Grand Saint-Bernard and Kredarica are actually "E"-type of climate (maximum monthly mean temperature below 10 °C). Table 2 indicates that all these stations located above 1000 m of altitude are classified as "Cb" (Oceanic) according to our classification, due to their low Hölder exponents. Such a result may seem surprising at first sight but is discussed in Sect. 5.

4.3. *Comparison Between ECA&D and NCEP Data*

It can be asked whether the results described above are dependent on the dataset used (i.e., ECA&D, http://ecad.eu). To answer that question, we perform the same analysis on surface air temperature data from the NCEP/NCAR Reanalysis Project (http://www.esrl.noaa.gov/). In this dataset, our area of interest is divided in 27 x 10 pixels (1.875° of latitude, 1.905° of longitude), each of them associated with a signal of daily mean temperatures over the period 1951–2003. Figure 11 shows how Europe is divided in pixels, which are colored according to the mean temperature over the 53 years of data.

After removing the pixels corresponding to the different seas, we analyze the Hölder regularity and norm of the remaining air temperature profiles of the data using the wavelet leaders method. We then associate two climates to each pixel: one based on the Köppen–Geiger classification, the other one

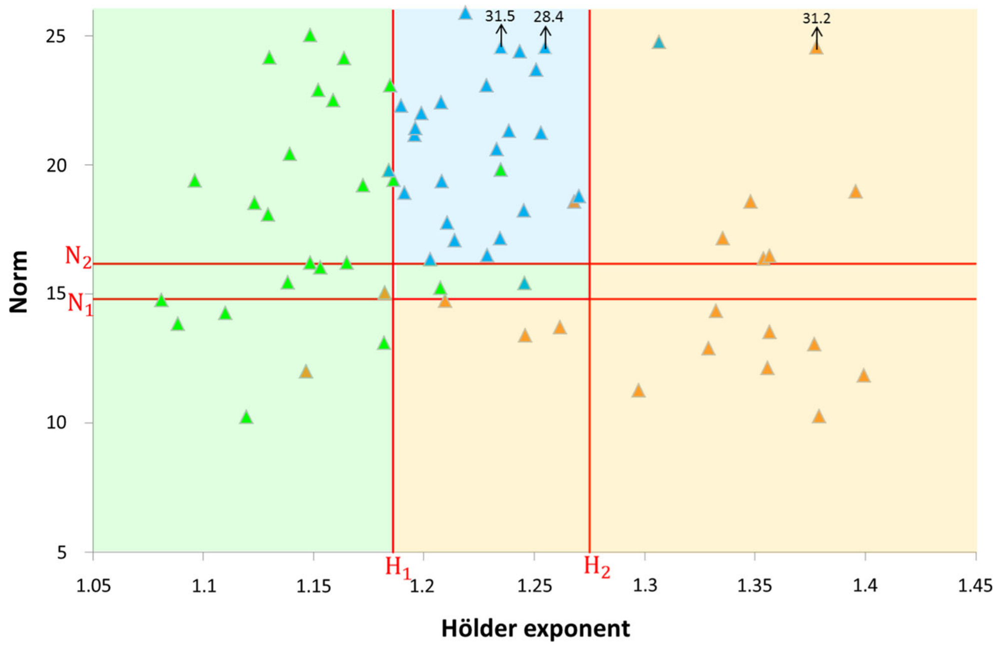

Figure 9
The *triangles* (*green* Cb, *orange* Ca, *blue* D) represent the distribution of the Hölder exponents and norms of the 69 weather stations selected for the blind test. In order to check if the classification based on the Hölder exponents and norms still match with Köppen's, the cut-out of the plane is left unchanged. Again, most of the points (almost 89 %) have the same color as the *rectangle* in which they are located, which confirms the first result

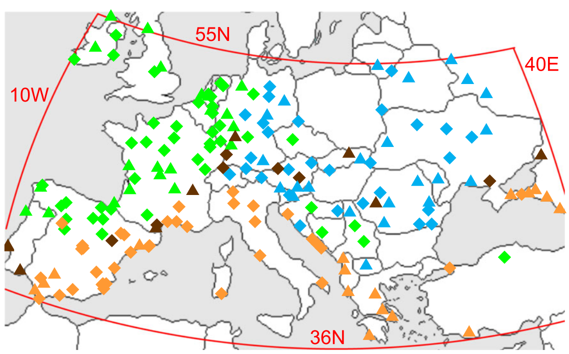

Figure 10
The first 115 weather stations are represented with *diamonds*, the 69 stations used for the blind test are represented with *triangles*. Each of them is colored as follows: oceanic stations (Cb-type) in *green*, continental stations (D-type) in *blue*, Mediterranean stations (Ca-type) in *orange*, and *brown diamonds* and *triangles* are used for stations for which the climate type is erroneously predicted by the Hölder-based classification

using the Hölder-based classification (Table 1). With the same color code as usual, the resulting maps are represented in Fig. 12a, b and match for 72 % of the pixels.

To compare this result with those obtained from the ECA&D analysis, maps of the same format representing these latter are needed. We first quad the map of Fig. 10 to have the same pixels as the NCEP maps, then we associate two climates to each pixel (using Köppen and Hölder-based classifications). In the case where a pixel does not include a weather station, the Hölder exponents, norms, minimum and maximum monthly mean temperatures are kriged to allow the two climate classifications. The resulting maps are represented in Fig. 12c, d and match for 85 % of the pixels. It can also be noted that the Köppen-based maps (a) and (c) match for 78 % of the pixels.

5. *Discussion*

Let us now take a closer look at the results obtained in Sect. 4.2. First, a major observation that stands out from Fig. 7 is that that the type of climate influences the regularity of the air temperature data.

Table 2

List of the stations located above 1000 m of altitude

Country	City	T_{max}	T_{min}	Köppen	Höld. exp.	Norm	Presc. clim.	Altitude (m)
Austria	Sonnblick	2.122	−12.65	Db	1.122618	20.834279	Cb	3106
Croatia	Zavizan	13.078	−4.0592	Db	1.136783	21.780321	Cb	1594
France	Mont Aigoual	12.901	−1.940	Db	1.12485	23.418699	Cb	1567
Germany	Fichtelberg	12.148	−4.712	Db	1.136309	20.456254	Cb	1213
Slovenia	Kredarica	6.493	−8.147	Db	1.097985	23.209143	Cb	2514
Slovenia	Vojsko	15.624	−2.577	Db	1.168453	16.368326	Cb	1067
Spain	Navacerrada	16.176	−0.728	Db	1.148477	19.520043	Cb	1894
Switzerland	Gd.-St.Bernard	7.576	−7.895	Db	1.130076	23.067411	Cb	2472
Switzerland	Säntis	5.927	−8.009	Db	1.077356	19.614025	Cb	2502
Ukraine	Ai-Petri	15.628	−3.346	Db	1.163423	19.520055	Cb	1180

Note that they are all classified as "Cb" because of their low Hölder exponent. This result seems surprising considering their Köppen–Geiger climate type; this is discussed in Sect. 5

Indeed, it appears that Oceanic stations display the lowest Hölder exponents, Continental stations have intermediate values of H, and Mediterranean stations have the largest. This implies that, from a daily point of view, Oceanic climate is more irregular, less stable than the two others, while the Mediterranean one is the most regular, the less variable in some way. It is an interesting fact that a method which does not use mean temperatures matches the Köppen–Geiger classification. It shows that the WLM is powerful enough to give results about a rather complex mathematical notion that are in good agreement with the intuition that surface air temperature variability is greater in Oceanic regions, whereas consecutive days are more likely to have the same air temperature in the South part of Europe. This could be explained by the fact that this region is more influenced by stable anticyclonic conditions, whereas the West coast of Europe is more impacted by the North Atlantic Oscillation and is therefore more subject to powerful winds, cold or humid air streams. These tend to trail off while entering the land, such that continental weather is slightly more regular. Such natural parameters affect the variability of air temperature, which is the principal ingredient of the Köppen–Geiger classification in Europe. Similarly, we can see that the Hölder exponent is the most important factor in the Hölder-based classification. If one does not take the norm into account, keeping only columns 1 and 3 of Table 1, the classification depends only on H: Oceanic if $H < H_1$, continental if $H_1 < H < H_2$, Mediterranean if $H > H_2$. In this case, 89.6 % of the 115 stations of reference and 84.1 % of the 69 used for the confirmation test are still correctly associated with their climate type.

This brings us to the discussion about the stations that are not correctly associated with their Köppen climate type, which is the case for 7 out of the 115 initial stations (see Table 3). Except for Salzburg and Graz, these stations are located at the confluence of different climate types [see Fig. 10 and Peel et al. (2007)], which makes the climate more difficult to prescribe. As far as these two Austrian stations are concerned, an explanation could be found in the topography of the region. Located at the foot of the Alps, the climate of these stations (Db according to Köppen) is probably highly influenced by the presence of the mountains nearby and is therefore different from Db-stations in Eastern Europe, which are easily detected by our classification. A comparable analysis can be made about the stations used for the blind test. As seen in Fig. 9, 8 out of these 69 stations are not associated with their Köppen climate type (see Table 4). These errors can be explained by the same arguments as above. Perpignan (close to Carcassonne), Lyon, Mannheim and Rostov-on-Don are located in areas where different types of climates meet (see Fig. 10). Although it cannot be clearly seen in Fig. 10 due to the lack of stations in this region, Portugal undergoes both Oceanic and Mediterranean climate [see e.g., Peel et al. (2007)], hence the same explanation still holds for Tavira and Lisbon. On the other hand, the cases of Poprad and Deva are similar to Graz and Salzburg since the former is located at

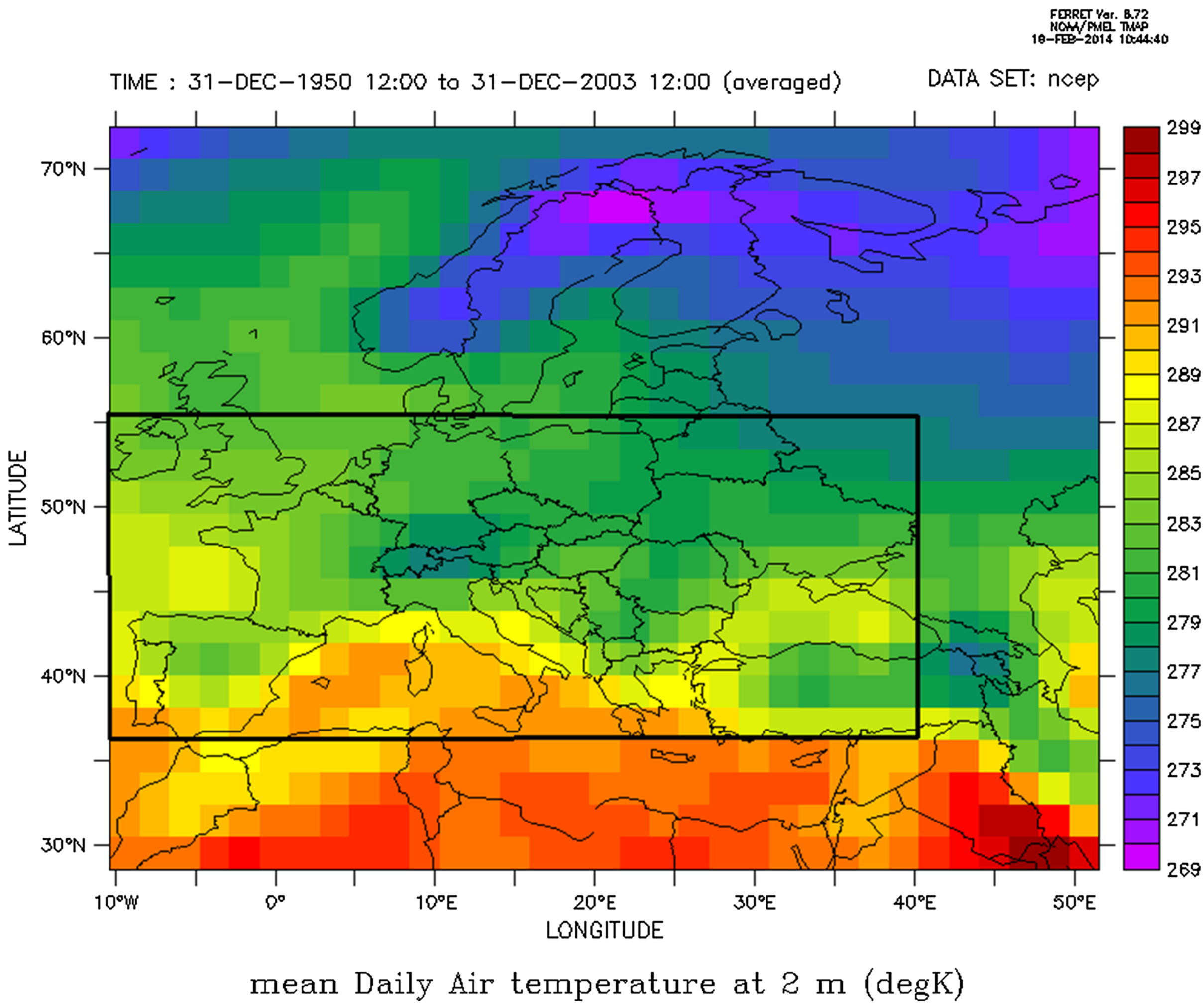

Figure 11

Illustration of the cut-out of Europe into pixels by the NCEP data; the area of interest is the region included in the *black box*. The *colors of the pixels* represent the mean temperature of the corresponding region over the period 1951 to 2003. Image provided by the NOAA-ESRL Physical Sciences Division, Boulder Colorado from their Web site at http://www.esrl.noaa.gov/psd/

the foot of the High Tatra Mountains and the latter is enclaved between the Apunesi Mountains and the Retezat Mountains in the Carpathian Mountains. Nonetheless, with a correspondence of 88.4 %, the excellent results obtained in the confirmation test validate the "Hölder-based classification". This is reinforced by the fact that most of these new stations are located in countries in which none of the first 115 stations were situated (e.g., Greece, Portugal, Russia, see Fig. 10).

The case of stations located above 1000 m of altitude is interesting since they are all classified as Oceanic due to their low Hölder exponents. It is important to note that, at high altitude, climate is more impacted by the variability from the free atmosphere induced by the general circulation and climate tends to be very irregular as the oceanic climate is. This feature, embodied by a decrease in the values of H with altitude, is detected with the wavelet leaders method. In addition, a closer examination at these stations reveals that 7 (out of 10) of them have a Hölder exponent lower than 1.137, which is smaller than 94 % of the stations of reference, and a norm higher than 19.6. Only 2 out of the 115 initial stations have such values for H and N. Therefore, it is reasonable to assert that our classification could be

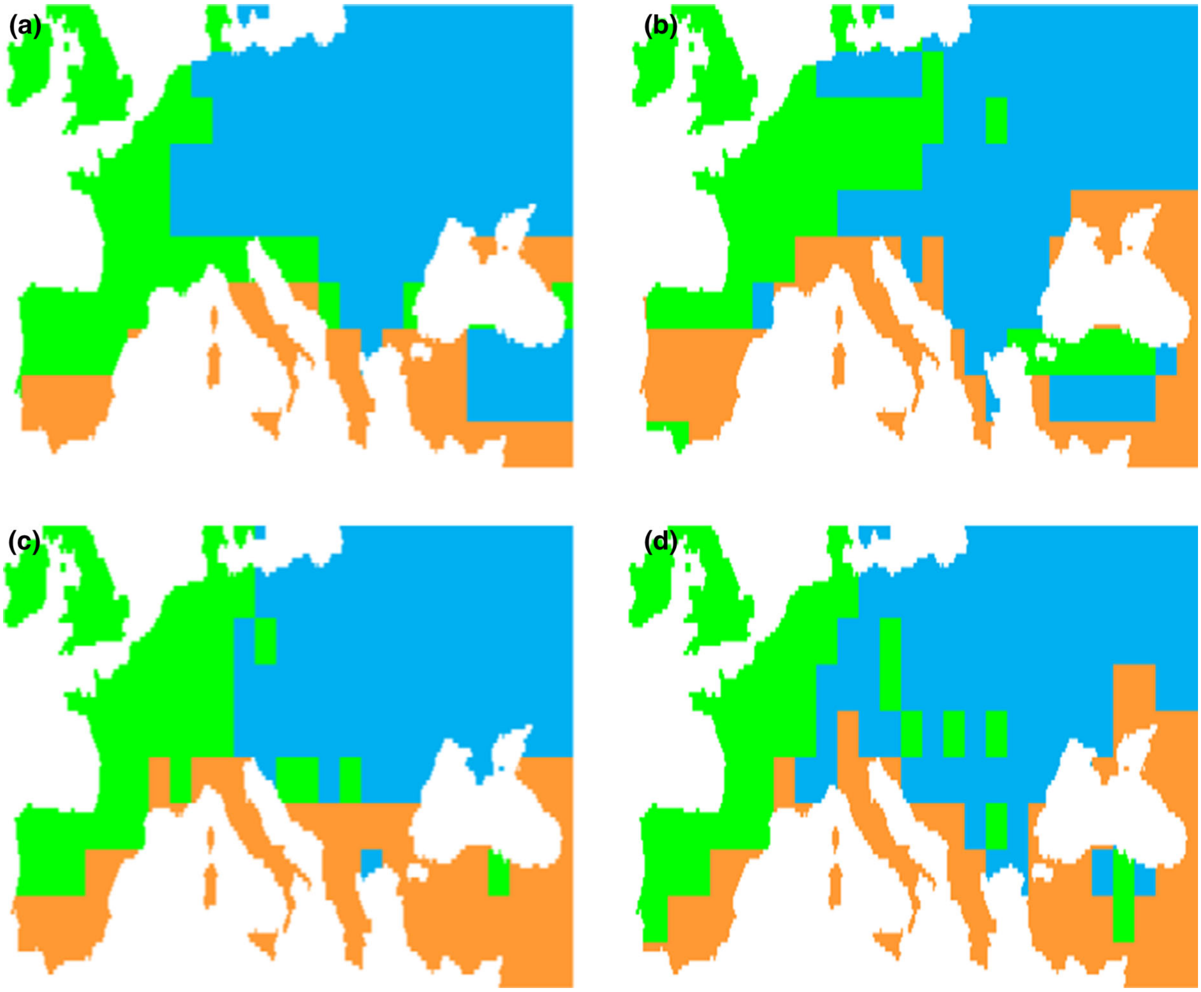

Figure 12
a (resp. **b**) Köppen (resp. Hölder)-based climate map obtained with the NCEP/NCAR dataset. The two maps match for 72 % of the pixels. **c** (resp. **d**) Köppen (resp. Hölder)-based climate map obtained with air temperature data from ECA&D. The maps match for 85 % of the pixels. Note that the Köppen maps **a** and **c** have a correspondence of only 78 %

enhanced by defining a mountain climate for stations having $H < 1.137$ and $N > 19.6$. Such a category could not have been guessed from the initial results and should be considered with caution due to the restricted number of stations above 1000 m at our disposal. Besides, among the 3 remaining ones, Navacerrada (Spain) is somehow a nonstandard high altitude location in Europe [see Peel et al. (2007)] and Vojsko and Ai Petri are those with the lowest altitude in this category (resp. 1067 and 1180 m). It is thus probable that the decrease in the value of H due to altitude is limited in their case.

Finally, we can comment on the results obtained with the NCEP dataset in Sect. 4.3. One can notice that the three types of climate are still well discernible and well located in Fig. 12. Also, it appears that the Köppen-Hölder correlation between (c) and (d) is higher than the Köppen NCEP-ECA&D correspondence between (a) and (c), which explains the relatively low correspondence percentage between the NCEP maps (a) and (b). However, the global tendencies remain visible and detectable with the NCEP/NCAR data, which emphasizes the independence of the results from the dataset and stresses the

Table 3

List of the weather stations for which the prescribed climate type and Köppen climate type do not match

Country	City	T_{max}	T_{min}	Köppen	Köp. 0.5 °C	Höld. exp.	Norm	Presc. clim.
Austria	Graz	19.77	−1.03	Db	Db	1.237392	14.855771	Cb
Austria	Salzburg	18.63	−1.14	Db	Db	1.183642	20.784577	Cb
France	Carcassonne	22.06	6.07	Ca	Cb	1.213563	17.911308	Db
France	Strasbourg	19.35	1.24	Cb	Cb	1.202237	19.530489	Db
Spain	Daroca	22.03	4.29	Ca	Cb	1.249235	17.536314	Db
Switzerland	Basel	19.26	1.2	Cb	Cb	1.203103	19.117983	Db
Ukraine	Askaniia Nova	22.8	−2.44	Da	Da	1.384888	21.832402	Ca

T_{max} and T_{min} correspond to the maximum and minimum monthly mean temperatures (in Celsius degrees), defining the Köppen climate type of the stations (column "Köppen"). Column "Köppen 0.5 °C" corresponds to the other possible climate types that can be associated with the stations close to 0.5 °C of these climates. The values of Hölder exponents and norms give the prescribed climate of the stations following our classification

Table 4

List of the weather stations (among the 69 used for the blind test) for which the prescribed climate type and Köppen climate type do not match

Country	City	T_{max}	T_{min}	Köppen	Köp. 0.5 °C	Höld. exp.	Norm	Presc. clim.
France	Lyon	20.912	2.826	Cb	Cb	1.234968	19.808594	Db
France	Perpignan	23.754	8.134	Ca	Ca	1.268003	18.592176	Db
Germany	Mannheim	19.705	1.434	Cb	Cb	1.186279	19.411953	Db
Portugal	Lisbon	22.784	11.362	Ca	Ca	1.146779	12.008029	Cb
Portugal	Tavira	23.72	11.377	Ca	Ca	1.182189	15.055671	Cb
Romania	Deva	22.275	−1.896	Da	Db	1.245781	15.431212	Cb
Russia	Rostov-on-Don	23.289	−4.116	Da	Da	1.306657	24.74907	Ca
Slovakia	Poprad	15.847	−4.77	Db	Db	1.184195	19.800468	Cb

T_{max} and T_{min} correspond to the maximum and minimum monthly mean temperatures (in Celsius degrees), defining the Köppen climate type of the stations (column "Köppen"). Column "Köppen 0.5 °C" corresponds to the other possible climate types that can be associated with the stations close to 0.5 °C of these climates. The values of Hölder exponents and norms give the prescribed climate of the stations following our classification

fact that surface air temperature variability, through Hölder exponents, is correlated to the climate types in Europe.

6. Conclusion and Future Work

In conclusion, we first show that the Hölder exponents from surface air temperature data in Europe are anti-correlated to the associated standard deviation of pressure anomalies. Then, we establish a climate classification based on these Hölder exponents that allows to recapture the renowned Köppen–Geiger climate classification. It appears that Oceanic stations display the lowest Hölder exponents, Continental stations have intermediate exponents, and Mediterranean stations have the largest. We perform a blind test to verify the efficiency of our classification and we investigate the particular nature of stations located at high altitude. The computations performed with another dataset confirm that, as quantified by notion of the Hölder exponent, temperature variability is correlated to climate types in Europe.

The results presented in this paper, as well as the method used, could be useful to test and compare different climate models. It could help in the detection of abnormalities in reanalyses or could indicate if some factors tend to "smoothen" the temperature curves. Apart from these potential impacts in climate modeling and, to some extent, to weather forecast, the issue of a generalization to other parts of the world can be considered. Indeed, the discussion about stations placed at high altitude raises the question of the detection of completely different types of climates, such as Tropical, Dry, or Polar climates. Of course, the current version of the Hölder-based classification is not able to detect them provided that it is calibrated for Europe and that we do not know which part of the (H, N) plane they would occupy. It is possible that they are not clearly discernible from some European climates from a Hölder point of view. However, is it really relevant to try to contrast the Hölder exponents of Madrid and of Brasilia if they accidentally lie close to each other in the (H, N) plane? Maybe they have a similar regularity although Brasilia is globally wetter and hotter, so that there would be actually no mistake by placing them in the same area of the plane. The real interesting problem would be to establish a Hölder-based classification specific, for e.g., South America that is able to distinguish the different types of climates present in that particular consistent geographic area. In line with this example, we could imagine that the impact of precipitation on daily temperatures could be observed in data from this region, while it is not the case in Europe. Moreover, it is always possible to add new features in relation with H and N if we really want to ramify our classification. Indeed, it may be good to recall that the Köppen–Geiger classification uses a dozen of indicators related to temperature and precipitation to distinguish 34 types of climates. Be that as it may, the results obtained for Europe are more than encouraging and there is clearly an exciting challenge ahead with the study of other continents and with the prospect of mapping the world according to the Hölder regularity of surface air temperature data.

Acknowledgments

We acknowledge the data providers in the ECA&D project (Tank et al. 2002) (data and metadata available at http://ecad.eu) and in the NCEP/NCAR Reanalysis Project (GHCN Gridded V2 data were provided by the NOAA-OAR-ESRL PSD, Boulder, Colorado, USA, from their Web site at http://www.esrl.noaa.gov/). We also thank the two anonymous reviewers for their constructive comments, which helped us to improve the manuscript.

References

Abry, P., Wendt, H., Jaffard, S., Helgason, H., Goncalves, P., Pereira, E., Charib, C., Gaucherand, P., & Doret, M. (2010). Methodology for multifractal analysis of heart rate variability: from lf/hf ratio to wavelet leaders. In Nonlinear Dynamic Analysis of Biomedical Signals EMBC conference (IEEE Engineering in Medicine and Biology Conferences).

Allaart, P. C., & Kawamura, K. (2011). The Takagi function: a survey. *Real Analysis Exchange*, *37*(1), 1–54.

Arneodo, A., Bacry, E., Graves, P. V., & Muzy, J. F. (1995). Characterizing long-range correlations in DNA sequences from wavelet analysis. *Physical Review Letters*, *74*(16), 3293–3297.

Arneodo, A., Bacry, E., & Muzy, J. F. (1995). The thermodynamics of fractals revisited with wavelets. *Physica A*, *213*, 232–275.

Arneodo, A., Vaillant, C., Audit, B., Argoul, F., D'aubenton-Carafa, Y., & Thermes, C. (2011). Multi-scale coding of genomic information: from dna sequence to genome structure and function. *Physics Report*, *498*, 45.

Audit, B., Bacry, E., Muzy, J. F., & Arneodo, A. (2002). Wavelet-based estimators of scaling behavior. *IEEE Transactions on Information Theory*, *48*, 2938.

Daubechies, I. (1992). *Ten lectures on wavelets*. Philadelphia, PA: SIAM.

Jaffard, S. (2004). Wavelet techniques in multifractal analysis. *Proceedings of symposia in pure mathematics*, *72*, 91–152.

Jaffard, S., Lashermes, B., Abry, P. (2006). Wavelet leaders in multifractal analysis. In *Wavelet analysis and applications* (pp. 201–246). Basel, Switzerland: Birkauser.

Jaffard, S., & Nicolay, S. (2009). Pointwise smoothness of space-filling functions. *Applied and Computational Harmonic Analysis*, *26*, 181–199.

Köppen, W. (1936). *Das geographische system der klimate*. Berlin: Gebrüder Borntraeger.

Koscielny-Bunde, E., Bunde, A., Havlin, S., Roman, H. E., Goldreich, Y., & Schellnhuber, H.-J. (1998). Indication of a universal persistence law governing atmospheric variability. *Physical Review Letters*, *81*, 729–732.

Lashermes, B., Roux, S. G., Abry, P., & Jaffard, S. (2008). Comprehensive multifractal analysis of turbulent velocity using wavelet leaders. *The European Physical Journal B*, *61*(2), 201–215.

Mallat, S. (1999). *A wavelet tour of signal processing*. San Diego, CA: Academic Press.

Mandelbrot, B. B., & Van Ness, J. W. (1968). Fractional brownian motions, fractional noises and applications. *SIAM*, *10*(4), 422–437.

Riley, M. A., Bonnette, S., Kuznetsov, N., Wallot, S., Gao, J. (2012). A tutorial introduction to adaptive fractal analysis. *Frontiers in Physiology*, *3*, 371. doi:10.3389/fphys.2012.00371.

Muzy, J. F., Bacry, E., & Arneodo, A. (1994). The multifractal formalism revisited with wavelets. *International Journal of Bifurcation and Chaos*, *4*, 245.

Peel, M., Finlayson, B., & McMahon, T. (2007). Updated world map of the Köppen–Geiger climate classification. *Hydrology and Earth System Sciences*, *11*, 1633–1644.

Shidfar, A. (1986). On the continuity of the Van Der Waerden's function in the Hölder sense. *American Mathematical Monthly*, *93*(5), 375–376.

Sonechkin, D. M., & Datchenko, N. L. (2000). Wavelet analysis of nonstationary and chaotic time series with an application to the climate change problem. *Pure and Applied Geophysics*, *157*, 653–677.

Tank, K. (2002). Daily dataset of 20th-century surface air temperature and precipitation series for the European Climate Assessment. *International Journal of Climatology*, *22*, 1441–1453.

Tricot, C., et al. (1999). *Courbes et dimension fractale*. Berlin: Springer-Verlag.

Website. European climate assessment and dataset. http://ecad.eu. Accessed 24 Oct 2013.

Website. Ncep/ncar reanalysis project. http://www.esrl.noaa.gov/. Accessed 21 Feb 2014.

Wendt, H., Abry, P., Jaffard, S., Ji, H., & Shen, Z. (2009). *Wavelet leader multifractal analysis for texture classification*. In Proceedings of the IEEE conference on ICIP.

(Received September 5, 2015, revised June 15, 2016, accepted June 21, 2016, Published online July 1, 2016)